東北大学機関リポジトリ
TOUR
Tohoku University Repository

Engineering of Surface Environment of Pd Nanoparticle Catalysts on Carbon Support with Pyrene Thiol Ligands for Semihydrogenation of Alkynes

著者	Takeharu Yoshii, Daiki Umemoto, Yasutaka Kuwahara, Kohsuke Mori, Hiromi Yamashita
journal or publication title	ACS Applied Materials & Interfaces
volume	11
number	41
page range	37708-37719
year	2019-09-20
URL	http://hdl.handle.net/10097/00130896

doi: 10.1021/acsami.9b12470

Engineering of surface environment of Pd nanoparticle catalysts on carbon support with pyrene-thiol ligands for semi-hydrogenation of alkynes

Takeharu Yoshii,[†] *Daiki Umemoto,*[†] *Yasutaka Kuwahara,*[†,‡] *Kohsuke Mori,*[†,‡]

and Hiromi Yamashita[*,†,‡]

[†] Division of Materials and Manufacturing Science, Graduate School of Engineering, Osaka University, 2-1 Yamadaoka, Suita, Osaka 565-0871, Japan.

[‡] Elements Strategy Initiative for Catalysts & Batteries Kyoto University (ESICB), Kyoto University, Katsura, Kyoto 615-8520, Japan.

Corresponding Author

*E-mail: yamashita@mat.eng.osaka-u.ac.jp

Keywords: Pyrene-thiol ligands, Surface modification, Pd nanoparticles, Semi-hydrogenation, Heterogeneous catalysis

Abstract

A new type of pyrene-thiol-derivative-modified Pd nanoparticle (NP) catalyst on a carbon black support for the efficient semi-hydrogenation of alkynes to alkenes is reported herein. Colloidal Pd NPs surrounded by pyrene-thiol modifiers were prepared using the two-phase Brust method, followed by impregnation of carbon black materials. Based on the structural characterization of the prepared catalyst ($PyC_{12}S$-Pd/VC) by NMR, UV-vis, FT-IR, TEM, HAADF-STEM, Pd K-edge XAFS, XRD, N_2 adsorption and XPS, we show that highly dispersed Pd NPs are immobilized on the catalysts *via* π-π interaction between pyrene groups bounded to the Pd NPs and carbon black supports. $PyC_{12}S$-Pd/VC efficiently catalyzes the alkyne semi-hydrogenation reaction while maintaining high alkene selectivity; an alkene selectivity of 94% is attained at 98% conversion after 5 h of reaction, and the selectivity was retained around 80% during 10 h of reaction. This performance is superior to that of a catalyst without pyrene groups and that of a commercial Lindlar catalyst. The steric hindrance of pyrene groups restricts access by the substrates to Pd NP surfaces, suppressing the unfavorable over-hydrogenation of alkenes to alkanes, which is revealed by the solvent and substrate dependency on the catalytic performance and DFT calculation study. Furthermore, the high selectivity and stability of $PyC_{12}S$-Pd/VC are caused by the strong interaction between pyrene groups and carbon supports, which prevents the separation of pyrene modifiers and the leaching or sintering of Pd NPs during the catalytic reaction. It is demonstrated that the combination of Pd NPs, pyrene-thiol modifiers, and carbon supports offers high activity, alkene selectivity, and stability in the semi-hydrogenation reaction.

Introduction

The semi-hydrogenation of alkynes to corresponding alkenes is a highly important reaction in the field of industrial materials and fine chemicals synthesis.[1,2] Among reported transition-metal catalysts, Pd catalysts are the most effective for the semi-hydrogenation of alkynes due to their balance of activity and selectivity.[3-5] Lindlar catalysts (5 wt.% Pd deposited on $CaCO_3$ treated with Pb salts) are the most widely utilized catalyst type for the semi-hydrogenation of alkynes, where Pd nanoparticles (NPs) are modified with Pb and basic additives such as quinoline to inhibit the over-hydrogenation of produced alkenes to alkanes.[6,7] Unfortunately, the requirement of highly toxic Pb salts and quinoline is a serious drawback. Moreover, although Lindlar catalysts are effective for the semi-hydrogenation of internal alkynes, terminal alkynes frequently suffer from over-hydrogenation to alkanes, resulting in low alkene selectivity.[8-10] Therefore, an alternative hazardous-additive-free catalyst for the semi-hydrogenation of terminal alkynes is desired.

Various types of catalyst for semi-hydrogenation that overcome the drawbacks of Lindlar catalysts have been developed.[11-15] In particular, Pd NP catalysts modified with organic compounds, such as amine, thiol, or phosphate, have attracted attention as substitutes for Lindlar catalysts, in which strongly coordinated N, S, or P atoms on the Pd surface control the adsorption kinetics of the produced alkenes, resulting in high alkene selectivity.[16-19] Organic ligands have been reported to play two roles in attaining high selectivity: (1) they constrain access by substrates and products to the metal surfaces (geometric effect), and (2) they reduce hydride coverage at the metal surfaces (electronic effect).[11,20,21] To maximize these geometric and electronic effects in organic-ligand-modified NP catalysts, the precise control of the size, shape and structure of NPs is crucial. Therefore, colloidal methods, rather than typical impregnation techniques, are frequently employed for the preparation of such catalysts.[22-24] However, insufficient modifier-metal bindings

and modifier-support interactions, inherent for colloidal preparation methods, lead to the separation of modifiers from NPs as well as leaching or sintering of NPs during the catalytic reaction, resulting in poor catalytic stability and product selectivity. Therefore, the optimization of the combination of organic modifiers, metals and supports is a crucial factor for developing high-performance catalysts. Catalysts for hydrogenation reaction with sufficient stability have recently been strongly desired in many fields such as Bio-Fuel upgrading, and the development of highly durable catalysts would be applicable in such fields. [25-27]

In molecular electrocatalysis, pyrene, a polycyclic aromatic hydrocarbon, is extensively employed as a noncovalent anchor for catalyst fixation on carbon materials.[28-30] Various types of pyrene complex and enzyme conjugate have been synthesized and immobilized on carbon nanotubes and carbon black materials with the aid of π-π interactions; these compounds show both high electrocatalytic activity and chemical stability.[31-33] Recently, pyrene-tethered Au or Pt NPs on carbon materials have been synthesized as a new type of nanohybrid material.[34-36] These studies inspired us to utilize pyrene-thiol derivatives with carbon materials as a macro-ligand for Pd NPs to suppress the separation and leaching of thiol-modifiers during the hydrogenation reaction.

In this study, we fabricate well-defined pyrene-thiol-modified Pd NP catalysts on carbon black supports that are efficient in the semi-hydrogenation of terminal alkynes while maintaining high alkene selectivity. These catalysts outperform a catalyst prepared without pyrene groups and a commercial Lindlar catalyst. Experiments and calculations suggest that the unfavorable over-hydrogenation of alkenes to alkanes is inhibited due to the steric hindrance of pyrene groups. In addition, the strong interaction between pyrene groups and carbon black supports efficiently suppresses the leaching of pyrene modifiers from the Pd NP surfaces and the aggregation of Pd

NPs during the catalytic reaction, resulting in high alkene selectivity, stability and reusability in the semi-hydrogenation reaction.

Experimental Section

Materials

1-bromopyrene, 4-hydroxy-phenylboronic acid, tripotassium phosphate (K_3PO_4), potassium carbonate (K_2CO_3), sodium sulfate (Na_2SO_4), sodium borohydride ($NaBH_4$), 1-dodecanethiol ($C_{12}SH$), anhydrous tetrahydrofuran (THF), anhydrous N,N-dimethylformamide (DMF), dichlroromethane (CH_2Cl_2), sodium chloride (NaCl), acetonitrile, disodium tetrachloropalladate(II) (Na_2PdCl_4), petroleum ether, methanol, hydrochloric acid (HCl), diethyl ether, toluene, styrene, ethylbenzene, biphenyl, dichloromethane, and quinoline were purchased from Nacalai Tesque Inc. S-(11-bromoundecyl)ethanethioate, tetraoctylammonium bromide (TOAB), diphenylacetylene, and fumed silica (SiO_2) were purchased from Sigma-Aldrich Co. LLC. Tetrakis(triphenylphosphine)palladium(0), phenylacetylene, and 1-phenyl-1-propyne were purchased from Tokyo Chemical Industry Co., Ltd. Vulcan XC-72 (VC), Ketjen black (KB), and Shirasagi M activated carbon (AC) were obtained from Cabot Corporation, Lion Specialty Chemicals Co., Ltd., and Osaka Gas Chemicals, respectively, as catalytic supports. Palladium-activated carbon (Pd 5%) (Pd/C) and palladium/calcium carbonate poisoned with lead (Pd 5%) (Lindlar catalyst) were purchased from Wako Pure Chemical Ind. Co., Ltd and Merck, respectively, as reference catalysts. Chloroform-D containing 0.03 % tetramethylsilane (TMS) was purchased from EURISO-TOP for ^1H NMR measurements. All chemicals were used as received without further purification.

Synthesis of pyrene-thiol ligand ($PyC_{12}SH$)

The pyrene-thiol ligand $PyC_{12}SH$ was synthesized based on a previously reported procedure (Scheme S1).[37] In the first step, 4-(pyrene-1-yl)phenol (**1**) was synthesized *via* a coupling reaction between 1-bromopyrene and 4-hydroxy-phenylboronicacid. 1-bromopyrene (1.00 g, 3.58 mmol) was dissolved in Ar-saturated anhydrous THF (30 mL). 4-hydroxy-phenylboronic acid (0.50 g, 3.58 mmol), tetrakis(triphenylphosphine)palladium(0) (40 mg) and K_3PO_4 (1.52 g) were added to the solution. After 20 h of stirring at 85 °C in an oil bath, the suspension was diluted with dichloromethane (50 mL) and extracted with NaCl-saturated H_2O (50 mL) twice. The organic phase was dried using Na_2SO_4 and purified using column chromatography (petroleum ether/CH_2Cl_2 = 1/1) to obtain compound **1**. ^{1}H NMR (396 MHz, $CDCl_3$) δ (ppm) = 8.26-7.90 (9H, m), 7.58-7.44 (2H, d, J = 7.9 Hz), 7.07-6.97 (2H, d, J = 8.3Hz).

Subsequently, S-(11-(4-(pyrene-1-yl)phenoxy)undecyl)ethanethioate (**2**) was synthesized using a nucleophilic substitution reaction with compound **1** and S-(11-bromoundecyl)ethanethioate. Compound **1** (0.10 g, 0.34 mmol) and K_2CO_3 (0.142 g) were dissolved in Ar-saturated anhydrous DMF (30 mL). S-(11-bromoundecyl)ethanethioate (0.628 mL, 1.02 mmol) was added to the suspension. After 24 h of reaction at 100 °C in an oil bath, the suspension was cooled to room temperature, diluted with dichloromethane (30 mL), and extracted with NaCl-saturated H_2O (50 mL) three times. The organic phase was dried using Na_2SO_4 and purified using column chromatography (petroleum ether/CH_2Cl_2 = 1/1) to obtain compound **2**. ^{1}H NMR (396 MHz, $CDCl_3$) δ (ppm) = 8.23-7.94 (9H, m), 7.57-7.50 (2H, d, J = 8.7 Hz), 7.13-7.03 (2H, d, J = 8.3 Hz), 4.11-4.00 (2H, m), 2.89-2.83 (2H, m), 2.34-2.30 (3H, s), 1.91-1.80 (2H, m), 1.60-1.46 (17H, m).

Finally, compound **2** (83.6 mg) was dissolved in methanol (3.0 mL), and then HCl (35%, 0.19 mL) was added to the solution. After 12 h of stirring under reflux conditions, the suspension was diluted in H_2O (10 mL) and extracted using diethyl ether (3 × 10 mL). The solvent of the organic phase was dried to obtain 11-(4-(pyren-1-yl)phenoxy)undecane-1-thiol, which is denoted as $PyC_{12}SH$. ^1H NMR (396 MHz, $CDCl_3$) δ (ppm) = 8.22-7.91 (9H, m), 7.59-7.48 (2H, d, J = 8.7 Hz), 7.13-7.00 (2H, d, J = 7.9 Hz), 4.13-3.99 (2H, m), 2.60-2.44 (2H, m), 1.91-1.76 (2H, m), 1.43-1.17 (18H, m), 0.97-0.69 (4H, m).

Synthesis of pyrene-thiol-modified Pd NP colloids ($PyC_{12}S$-Pd NP colloids)

Pyrene-thiol-modified Pd NP colloids were prepared using the two-phase Brust method.[38] 0.184 mL of 20 mg/mL Na_2PdCl_4 aqueous solution (Pd: 12.5 μmol) and tetraoctylammonium bromide (TOAB, 10.3 mg) dissolved in toluene (1.25 mL) as a phase transfer catalyst were added into a glass reactor. After 5 min of stirring, $PyC_{12}SH$ (6.24 μmol, 3.0 mg) dissolved in toluene (0.5 mL) was added and stirred for 1 h at 30 °C. Subsequently, a freshly prepared $NaBH_4$ aqueous solution (4.7 mg in 0.5 mL of H_2O) was quickly added to the suspension and stirred for 3 h at 30 °C. The produced dark-brown colloids in the organic phase were centrifuged and washed with acetonitrile twice, and finally dispersed in 12.5 mL of dichloromethane to obtain dark-brown Pd NP colloids (Pd: 106.4 mg/mL), which are denoted as $PyC_{12}S$-Pd NP colloids. In addition, $C_{12}S$-Pd NP colloids were synthesized by a similar procedure using 1-dodecanethiol ($C_{12}SH$) instead of $PyC_{12}SH$ as a reference catalyst. No sedimentation was observed in any colloidal solutions, even after 1 month.

Synthesis of carbon-supported $PyC_{12}S$-Pd NP catalysts ($PyC_{12}S$-Pd/VC)

A catalyst was prepared using the impregnation method. 9.4 mL of $PyC_{12}S$-Pd NP colloid (Pd: 9.4 μmol) and 99 mg of Vulcan-XC72 (VC) were added in dichloromethane (40 mL) and ultrasonicated for 30 min. After 30 min of stirring, the solvent was dried using a rotary evaporator to obtain carbon-supported $PyC_{12}S$-Pd NP catalysts, which are denoted as $PyC_{12}S$-Pd/VC. To obtain the reference catalyst $C_{12}S$-Pd/VC, a synthesis was performed using $C_{12}S$-Pd NP colloid instead of $PyC_{12}S$-Pd NP colloid. Reference catalysts with different supports were synthesized using a similar procedure; Vulcan-XC72 (VC) was replaced with fumed silica (SiO_2), Ketjen black (KB), and Shirasagi M activated carbon (AC), respectively.

Characterization

^1H NMR spectra were obtained on a JEOL JNM-ECS 400 spectrometer operated at 400 MHz with $CDCl_3$ as a solvent and the tetramethylsilane (TMS) peak used as a reference. Powder X-ray diffraction (XRD) patterns were recorded using a Rigaku Ultima IV diffractometer with Cu Kα radiation (λ = 1.54056 Å). Transmission electron microscopy (TEM) images were obtained using a Hitachi Hf-2000 field emission-transmission electron microscope operated at 200 kV. Scanning transmission electron microscopy (STEM) images were obtained using a JEOL-ARM 200F operated at 200 kV. Ultraviolet-visible (UV-vis) absorption spectra were obtained using a Shimadzu UV-2600 UV-vis spectrophotometer with a quartz cell (light path length: 10 mm) at room temperature. Pd K-edge X-ray absorption fine structure (XAFS) spectra were recorded in fluorescence mode at 01B1 beamline at the SPring-8, JASRI, Harima, Japan (proposal nos. 2018B1082 and 2018B1185), using a Si(111) monochromator. The Fourier transform was applied

to the k^3-weighted normalized extended X-ray absorption fine structure (EXAFS) data over the range of $3.0 < k$ (Å^{-1}) < 12 to obtain radial structure functions using a Rigaku software REX2000. X-ray photoelectron spectroscopy (XPS) was performed with a Shimadzu ESCA-3400 XPS system using the Mg Kα line (1253.6 eV). The binding energy was calibrated using the C 1s photoelectronic peak at 284.5 eV. N_2 adsorption isotherms were obtained by using a MicrotracBEL Corp. BELsorp-max system at -196 °C. The Brunauer-Emmett-Teller (BET) surface area was calculated using a multipoint BET method from the adsorption data in the range of $p/p_0 = 0.05$-0.25, and the mesopore volume (V_{meso}; pore diameter: 2-50 nm) was calculated from Barrett-Joyner-Halenda (BJH) plots. Fourier transform-infrared (FT-IR) spectra were measured on a JASCO FT/IR-6300 instrument under vacuum using samples diluted with KBr. Temperature-programmed desorption (TPD) was carried out using a MicrotracBEL Corp. BELCATII instrument by heating a 10 mg sample at 5 °C/min up to 900 °C under a 30 mL/min He flow.

Catalytic test

The catalytic performance in the semi-hydrogenation of phenylacetylene was evaluated.[3] In a typical procedure, a suspension containing dichloromethane (10 mL), biphenyl (38.6 mg, 0.25 mmol) as an internal standard, and the catalyst (5 mg) were added into a glass reactor. The reactor was placed in an oil bath at 30 °C, and hydrogen gas (10 mL min^{-1}) was bubbled through the suspension for 30 min prior to the reaction. The reaction was initiated by the injection of an alkyne (0.5 mmol) into the reactor using a syringe under 10 mL min^{-1} hydrogen bubbling and continuous stirring. Products were analyzed using gas chromatography (Shimadzu, GC-2014) with a frame ionization detector (FID) and a non-polar capillary column (TC-1, 60 m × 0.32mm × 0.25 μm). When the commercial Lindlar catalyst was used, 5 mol% quinoline was added into the reaction

suspension and heptane (10 mL) was used as a reaction solvent following a previous report.[7,15] In a competing reaction of internal and terminal alkynes, a mixture of phenylacetylene (0.25 mmol) and diphenylacetylene (0.25 mmol) was used as a substrate in the above procedure. An NP leaching test was performed using a hot filtration process with a membrane filter after 2 h of reaction. In a reusability test, the used catalyst was recovered by centrifugation, washed with dichloromethane, and then subjected to several catalytic cycles. The leaching rate of the pyrene-thiol ligands during the catalytic reaction was estimated as follows. A suspension containing dichloromethane (10 mL) and the catalyst (5 mg) was added to the glass reactor, and hydrogen gas (10 mL min^{-1}) was bubbled through the suspension for 6 h. The resultant suspension was filtered, and the filtrate was analyzed using UV-vis measurements in the wavelength range of 300-400 nm to detect the presence of pyrene groups. For $PyC_{12}S$-Pd NP colloidal catalysts, a centrifugation process was employed instead of filtration in the above procedure for the removal of the catalyst from the suspension.

DFT calculation

All density functional theory (DFT) calculations were performed using the $DMol^3$ program in Materials Studio 17.2.[39,40] The generalized gradient approximation (GGA) exchange-correlation functional proposed by Perdew, Burke and Ernzerhof (PBE) was combined with the double numerical basis set plus polarization functions (DNP). The PBE functional was utilized with dispersion correction using the Tkatchenko-Scheffler (TS) scheme.[41] (i) A pyrene-thiol ligand ($PyC_{12}SH$) immobilized on (3×2) Pd (111) surface cell and (ii) a dodecanethiol ligand ($C_{12}SH$) immobilized on (3×2) Pd (111) surface cell were employed for the surface model of $PyC_{12}S$-Pd NPs and $C_{12}S$-Pd NPs. The bottom two Pd layers were fixed at the corresponding bulk position,

and the top Pd layer and the ligands were allowed to relax during geometry optimizations. A vacuum spacing was set to 50 Å to avoid nonphysical electronic interaction. Simulated FT-IR spectra of molecular $PyC_{12}SH$ and $C_{12}SH$ were obtained by the vibration analysis.

Results and discussion

Synthesis and characterization of $PyC_{12}S$-Pd/VC

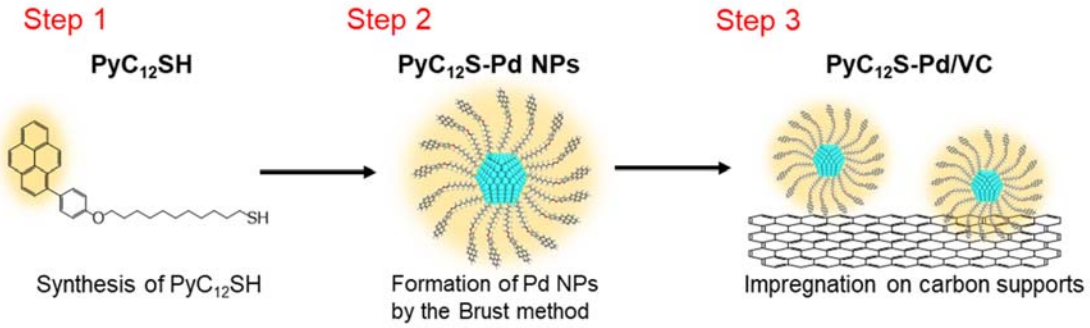

Scheme 1 Synthetic procedure of $PyC_{12}S$-Pd/VC.

Scheme 1 summarizes the synthetic procedure of $PyC_{12}S$-Pd/VC. In the first step, the pyrene- thiol ligand $PyC_{12}SH$ was synthesized *via* Suzuki-Miyaura coupling and a subsequent nucleophilic substitution reaction (Scheme S1). Successful synthesis of $PyC_{12}SH$ was confirmed by ^1H NMR measurement. The spectra of the intermediate products (**1**, **2**) and the final product of $PyC_{12}SH$ were fairly consistent with the reported ^1H NMR data (for details, see the experimental section and Figure S1).[37] These results are also supported by FT-IR and UV-vis measurements (see Figure S2 and S3).

In the next step, pyrene-thiol-modified Pd NP colloids ($PyC_{12}S$-Pd NP colloids) were prepared using the two-phase Brust method (Scheme 1, step 2).[38,42] $PyC_{12}SH$ dissolved in toluene and Na_2PdCl_4 aqueous solution were mixed in a molar ratio of Pd : $PyC_{12}SH$ = 2:1,[43] and stirred with TOAB as a phase transfer catalyst. Subsequently, $NaBH_4$ aqueous solution as a reducing agent was added to obtain $PyC_{12}S$-Pd NP colloids in the organic phase. 1-dodecanthiol-modified Pd NP colloids ($C_{12}S$-Pd NP colloids) were prepared using a similar procedure as the reference catalyst synthesis. Figures 1A and 1B show TEM images of $PyC_{12}S$-Pd NPs and $C_{12}S$-Pd NPs, respectively. Colloidal monodispersed NPs with mean diameters of 2.6 and 2.8 nm can be observed, respectively. In the FT-IR spectra (Figure 2A), $PyC_{12}SH$ shows a band at 3030 cm^{-1} due to the C-H stretching vibration and bands in the region of 1620 - 1500 cm^{-1} that can be assigned to the C-C stretches of aromatic rings, which are not seen in the case of $C_{12}SH$. $PyC_{12}S$-Pd NP and $C_{12}S$-Pd NP colloids both exhibit characteristic bands at 2852 cm^{-1} and 2921 cm^{-1} corresponding to the C-H stretching vibration of the alkyl chains.[43-45] Furthermore, the experimentally measured FT-IR spectra were in good agreement with the DFT simulated spectra (Figure S4). The UV-vis spectrum of $PyC_{12}SH$ (Figure 2B) shows three absorption bands at around 245, 280 and 350 nm, which are at the same position of those of 1-bromopyrene (see Figure S3).[36,37] $PyC_{12}S$-Pd NP colloid also show the UV-vis absorption similar to $PyC_{12}SH$, revealing the presence of pyrene groups even after the NP formation. These results indicate successful modification of the Pd NP surface with $PyC_{12}SH$ in $PyC_{12}S$-Pd NPs. To estimate a surface coverage of $PyC_{12}SH$ on Pd NPs, the amount of utilized $PyC_{12}SH$ was estimated by the UV-vis absorption difference of the reaction suspension before and after the Brust procedure (Figure S5A). Around 15.5% of the introduced $PyC_{12}SH$ was consumed in the modification of Pd NPs. If the cuboctahedral motif is employed for the model of Pd NPs, a Pd NP with a diameter of 2.6 nm corresponds to the 6-shell structure of 561 Pd atoms,

in which 252 Pd atoms are exposed to the surface (Figure S5B).[46,47] Based on this model, the surface coverage of $PyC_{12}SH$ is calculated to be 17.2% in $PyC_{12}S$-Pd NP colloids (for details, see supporting information), suggesting sufficient coverage of pyrene groups on the Pd NP surface.[48,49]

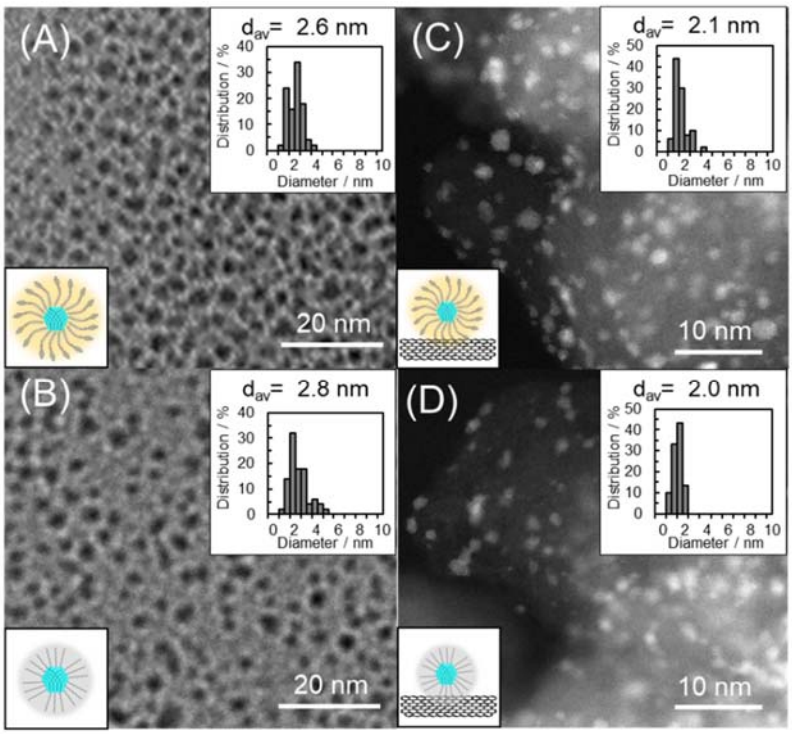

Figure 1 TEM images of (A) $PyC_{12}S$-Pd NP colloids, (B) $C_{12}S$-Pd NP colloids, and HAADF-STEM images of (C) $PyC_{12}S$-Pd/VC, (D) $C_{12}S$-Pd/VC. Inset in (A-D) shows a distribution diagram of the colloidal Pd NPs.

$PyC_{12}S$-Pd NP and $C_{12}S$-Pd NP colloids were supported on the carbon black Vulcan XC-72 using the impregnation method. The resulting catalysts are denoted as $PyC_{12}S$-Pd/VC and $C_{12}S$-Pd/VC, respectively (Scheme 1, step 3). HAADF-STEM images of $PyC_{12}S$-Pd/VC and $C_{12}S$-

Pd/VC (Figures 1C and 1D) show highly dispersed Pd NPs on the surface of the carbon black supports while maintaining the particle size of unsupported Pd NP colloids (Figures 1A and 1B). In addition, no aggregates can be observed in TEM images of $PyC_{12}S$-Pd/VC and $C_{12}S$-Pd/VC (Figures S6A and S6B). The high degree of dispersion of Pd NPs is supported by the XRD patterns for $PyC_{12}S$-Pd/VC and $C_{12}S$-Pd/VC, which have no peaks that can be assigned to the Pd crystal structure (typically at 40.0° and 46.6°) (Figure S7).[50] Figure S8 compares the N_2 adsorption/desorption isotherms and the corresponding BJH plots of $PyC_{12}S$-Pd/VC, $C_{12}S$-Pd/VC, and pristine VC. $PyC_{12}S$-Pd/VC and $C_{12}S$-Pd/VC have similar mesopore size distributions, where the pore volumes are lower than that for pristine VC in the pore diameter region of 2-6 nm. The Brunauer-Emmett-Teller (BET) specific surface area (S_{BET}) and the total mesopore volume (V_{meso}) (Table S1) of $PyC_{12}S$-Pd/VC and $C_{12}S$-Pd/VC are lower than those for pristine VC. These results indicate that well-dispersed Pd NPs with a diameter of 2-3 nm were immobilized in the mesopores of the carbon black supports in the prepared catalysts.[51,52]

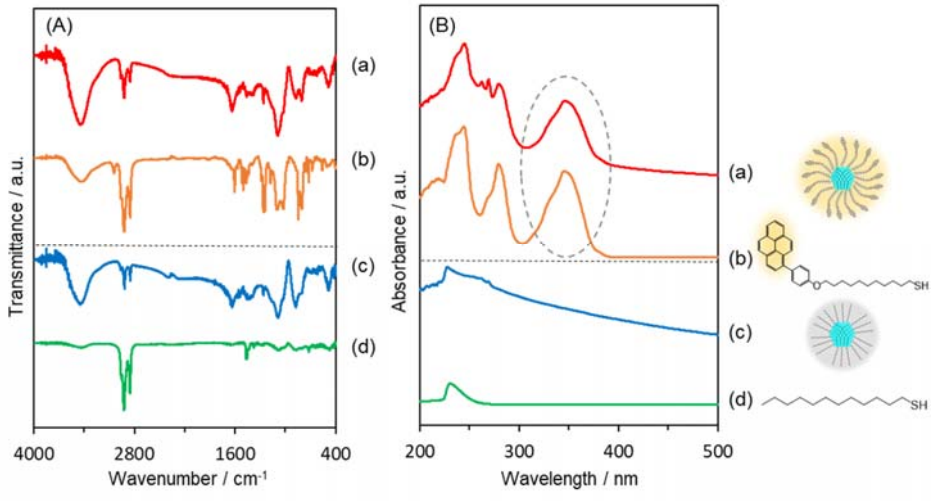

Figure 2 (A) FT-IR and (B) UV-vis spectra of (a) $PyC_{12}S$-Pd NP colloid, (b) $PyC_{12}SH$, (c) $C_{12}S$-Pd NP colloid, and (d) $C_{12}SH$.

To examine the state of Pd species on the carbon black, XAFS measurements were carried out. Figure 3 shows the Pd K-edge X-ray absorption near-edge spectra (XANES) and the Fourier-transformed extended X-ray absorption fine structure (EXAFS) spectra of the prepared catalysts and reference samples. The shapes of the XANES spectra of the prepared catalysts ($PyC_{12}S$-Pd/VC and $C_{12}S$-Pd/VC) are different from those of the reference samples (Pd foil and PdO). In addition, the absorption edges of the prepared catalysts are located between those for the Pd foil and PdO, suggesting that both Pd(0) and Pd(II) co-exist in the Pd NPs supported on the prepared samples.[16] The Fourier-transformed EXAFS spectra of $PyC_{12}S$-Pd/VC and $C_{12}S$-Pd/VC have distinct peaks at 1.8 and 2.5 Å; the first shell at 1.8 Å is assigned to the Pd-S bond, and the second shell at 2.5 Å is associated with the Pd-Pd bond.[47,53] These XANES and Fourier-transformed EXAFS spectra demonstrate that Pd NPs in $PyC_{12}S$-Pd/VC were definitely surrounded by the $PyC_{12}SH$ species even after being supported on the carbon supports. This is also confirmed by the detection of S species in $PyC_{12}S$-Pd/VC and $C_{12}S$-Pd/VC with S 2p XPS measurements (Figure S9).

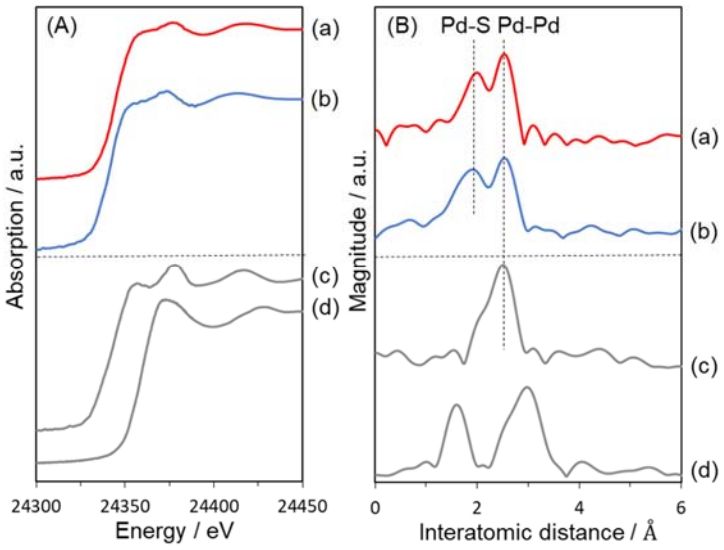

Figure 3 Pd K-edge (A) XANES spectra and (B) Fourier transformed EXAFS spectra of (a) $PyC_{12}S$-Pd/VC, (b) $C_{12}S$-Pd/VC and reference samples (c) Pd foil and (d) PdO.

Semi-hydrogenation of phenylacetylene

The catalytic performance of $PyC_{12}S$-Pd/VC was assessed in the semi-hydrogenation of phenylacetylene with bubbling of H_2 at 30 °C. This is a sequential reaction in which styrene (**4**), converted from phenylacetylene (**3**), is successively reduced to ethylbenzene (**5**) (Figure 4A). Figures 4B-E show the time courses in the semi-hydrogenation of phenylacetylene over the prepared catalysts ($PyC_{12}S$-Pd/VC and $C_{12}S$-Pd/VC) as well as a commercial carbon-supported Pd NP catalyst (Pd/C) and a Lindlar catalyst as references. When the prepared $PyC_{12}S$-Pd/VC was used as the catalyst, phenylacetylene was smoothly and selectively hydrogenated to styrene; 94% styrene selectivity was achieved at 98% conversion after 5 h of reaction. More importantly, the successive reduction of styrene to ethylbenzene was suppressed under H_2 bubbling after the conversion of phenylacetylene reached 100%, and the selectivity for styrene (red line in Figure 4B) was maintained at around 80% during 10 h of reaction. When $C_{12}S$-Pd/VC was used as the catalyst, the produced styrene was rapidly converted to ethylbenzene; the selectivity for styrene fell to 18% after 10 h of reaction. The commercial Pd/C catalyst was active for the hydrogenation of phenylacetylene, but its selectivity for styrene was quite low; the produced styrene was completely over-hydrogenated to the ethylbenzene after 6 h of reaction. Therefore, the prepared $PyC_{12}S$-Pd/VC efficiently inhibits over-hydrogenation to ethylbenzene, realizing the high selectivity for styrene. Furthermore, the commercial Lindlar catalyst with 5 mol% quinoline demonstrated 84% styrene selectivity at 100% conversion, but this selectivity rapidly decreased to 45% after 1 h of reaction thorough the over-reduction of styrene to ethylbenzene.

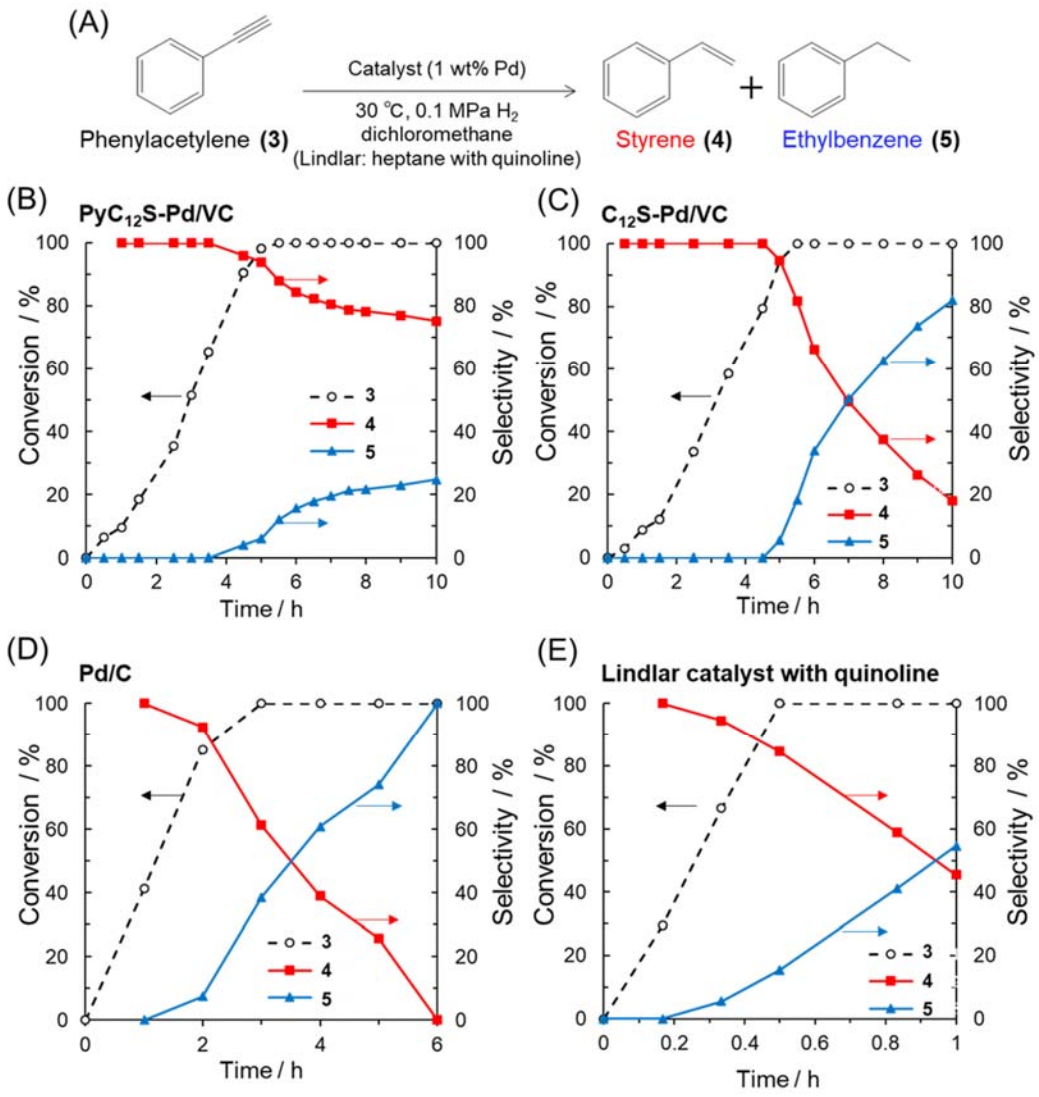

Figure 4 (A) Reaction scheme of the semi-hydrogenation of phenylacetylene, and time course in the semi-hydrogenation of phenylacetylene in dichloromethane over (B) $PyC_{12}S$-Pd/VC, (C) $C_{12}S$-Pd/VC and reference commercial catalysts (D) Pd/C and (E) Lindlar catalyst with quinoline.

The stability and reusability of $PyC_{12}S$-Pd/VC were investigated using leaching and reusability experiments. As shown in Figure 5A, the reaction was immediately quenched after the

removal of the catalyst by the hot-filtration process, revealing that the Pd NPs were steadily immobilized on the carbon black support during the catalytic reaction. Furthermore, no significant loss of activity or selectivity was observed in the reusability test over PyC$_{12}$S-Pd/VC (Figure 5B). It is noted that the slight decrease in activity in the 5th run is due to the loss of catalysts during the recycling experiments. TEM images of the catalyst after the reaction (Figures S10Ab and S10Ac) show that the high degree of dispersion of Pd NPs was retained and that the Pd NPs did not form aggregates. The XRD pattern of the catalyst after the reaction (Figure S11) does not show the peaks that can be assigned to the Pd crystal, suggesting no aggregation of Pd NPs during the reaction. In addition, the Pd 3d XPS spectra of PyC$_{12}$S-Pd/VC before and after the reaction were presented in Figure S12, and no significant change was shown in the binding energy peaks of Pd 3d even after the reaction. Considering these results, the prepared PyC$_{12}$S-Pd/VC shows high activity, selectivity, and stability for the semi-hydrogenation of terminal alkynes.

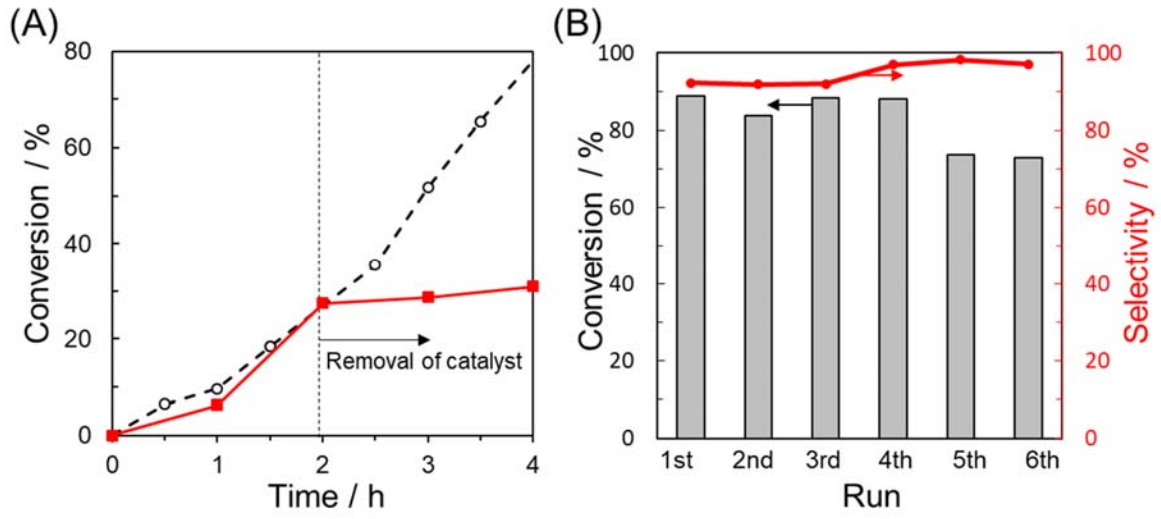

Figure 5 (A) Leaching test in the semi-hydrogenation of phenylacetylene over PyC$_{12}$S-Pd/VC. The red line represents the time course after the removal of the catalyst at 2 h. (B) Reusability test in the semi-hydrogenation of phenylacetylene over PyC$_{12}$S-Pd/VC.

Solvent-dependent reactivity switching over $PyC_{12}S$-Pd/VC in semi-hydrogenation

A study on the solvent dependence in the semi-hydrogenation reaction was performed to better understand the role of the pyrene functional groups in $PyC_{12}S$-Pd/VC. Figure 6 shows the catalytic performance in a non-polar solvent (toluene) and in a highly polar solvent (methanol) over the prepared catalysts. $C_{12}S$-Pd/VC shows nearly the same reaction profiles regardless of the reaction solvent (see Figures 4C, 6B and 6D), where phenylacetylene was first reduced to styrene, which in turn was rapidly reduced to ethylbenzene. In contrast, a quite different solvent dependence was exhibited by $PyC_{12}S$-Pd/VC. As shown in Figure 6A, the selectivity profile in toluene over $PyC_{12}S$-Pd/VC was similar to that over $C_{12}S$-Pd/VC (Figure 6B), where the sequential reduction of styrene to ethylbenzene was not suppressed. For the moderately polar solvent dichloromethane, over-hydrogenation was inhibited even after the conversion reached 100% as mentioned above (see Figure 4B). When the highly polar solvent methanol was used, $PyC_{12}S$-Pd/VC was completely inactive in the hydrogenation reaction even after 6 h of reaction (Figure 6C). Summarizing these results, specific reactivity switching was found for $PyC_{12}S$-Pd/VC, but not for $C_{12}S$-Pd/VC, depending on the solvent polarity, and therefore the pyrene groups in $PyC_{12}S$-Pd/VC affect catalytic reactivity. Previous studies have shown that the surrounding ligand environment, such as the ligand structure and conformation, depends on the reaction solvent and determines the overall activity and selectivity of NP catalysts.[54,55] For example, Pd NP colloidal catalysts surrounded by ligands containing carboxyl groups cause switching between hydrogenation and isomerization of allyl alcohol depending on the reaction solvent, where the conformation of the surrounding ligands is altered by the solvent polarity.[56] In the present study, the pyrene groups have a high affinity for non-polar solvents, and repel polar solvents. Figure S13 depicts the proposed conformation of the pyrene-thiol ligands on the Pd NP surface in the

respective solvents. In the non-polar solvent toluene, the pyrene-thiol ligands likely had an open structure due to the high affinity between pyrene and toluene, and therefore alkynes and alkenes could easily access the Pd NP surface, leading to low styrene selectivity. In the highly polar solvent methanol, the pyrene-thiol ligands likely fell toward the Pd NP surface and formed a closed structure due to the repulsion between pyrene and the solvent. Since neither alkenes nor alkynes were adsorbed on the Pd NP surface, completely no catalytic performance was observed in methanol. Finally, in the moderately polar solvent dichloromethane, the ligand structure was not be as open as that in toluene, but not completely closed, and therefore the substrates (alkynes and alkenes) were affected by the moderate steric hindrance of pyrene groups. Since the adsorption kinetics of alkenes on the Pd surface are weaker than that of alkynes,[57,58] it is conceivable that the steric hindrance of pyrene groups in dichloromethane prevents access to the Pd NP surface by alkenes and contributes to the suppression of over-hydrogenation, leading to high alkene selectivity.

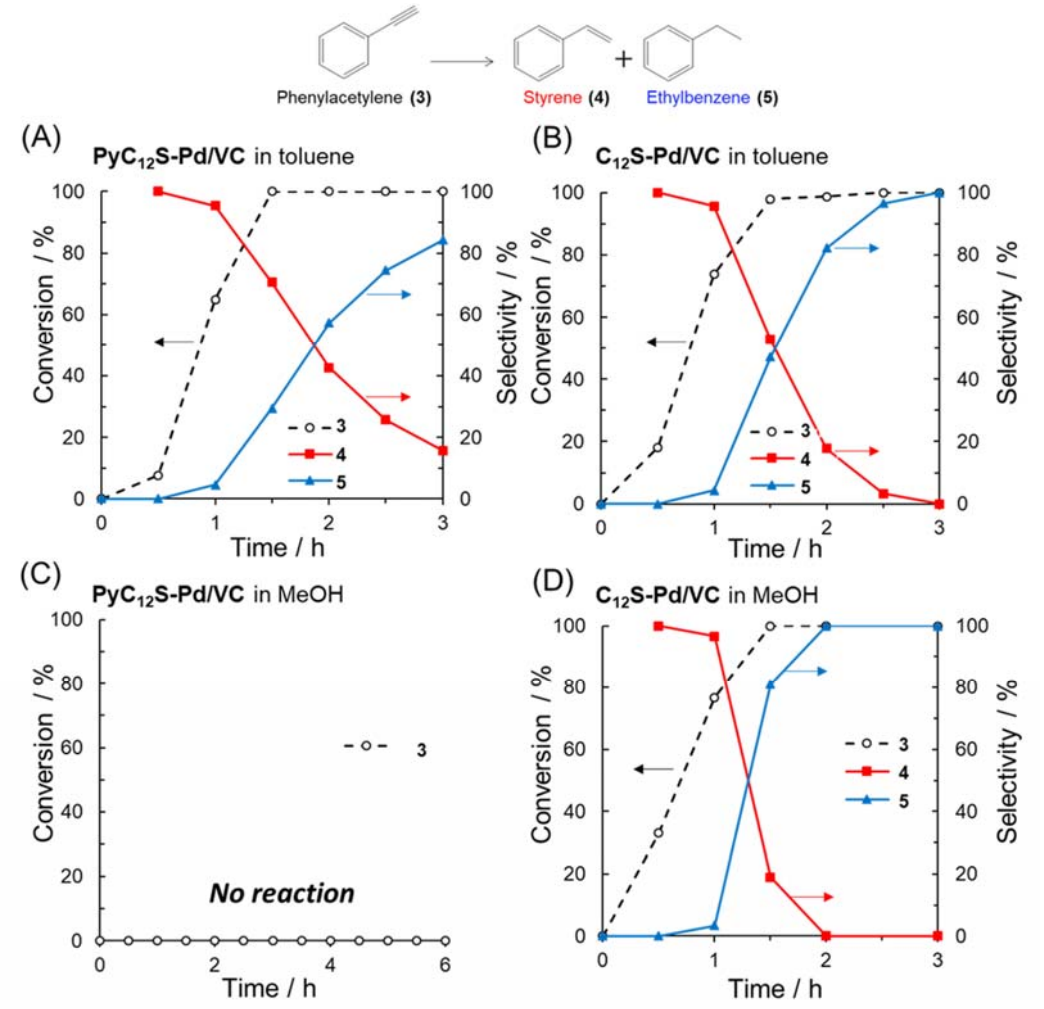

Figure 6 Time course in the semi-hydrogenation of phenylacetylene in toluene over (A) $PyC_{12}S$-Pd/VC and (B) $C_{12}S$-Pd/VC, and in methanol over (C) $PyC_{12}S$-Pd/VC and (D) $C_{12}S$-Pd/VC.

The density functional theory (DFT) calculations also demonstrate the crucial effect of the steric hindrance by pyrene groups. Pyrene-thiol ligands ($PyC_{12}SH$) and dodecanethiol ligands ($C_{12}SH$) fixed on Pd (111) surface cell were employed as models of $PyC_{12}S$-Pd/VC and $C_{12}S$-Pd/VC, respectively (Figure 7A and 7B). Based on the experimentally determined surface coverage of 17.2% (see Figure S5), the ligands were immobilized at a ratio of one to six surface Pd atoms in each calculation model. As shown in Figure 7A, the pyrene groups interact with each

other through π-π interaction, and the average interlayer distance between pyrene groups is 3.5 □, which is consistent with the interlayer spacing of π-π stacking in graphite (3.4 □).[59] In contrast, the average distance between ligands is 6.9 □ in the dodecanethiol fixed Pd surface model (Figure 7B). The size of the reaction substrates of phenylacetylene and styrene is estimated to be 4.3 × 7.6 □ (shown in Figure S14). Therefore, the access of the substrates should be restricted by the pyrene groups in $PyC_{12}S$-Pd/VC, while phenylacetylene can reach the Pd surface between ligands in $C_{12}S$-Pd/VC. These calculation results well explain the experimental observation that only $PyC_{12}S$-Pd/VC can prevent the over-hydrogenation, showing high styrene selectivity.

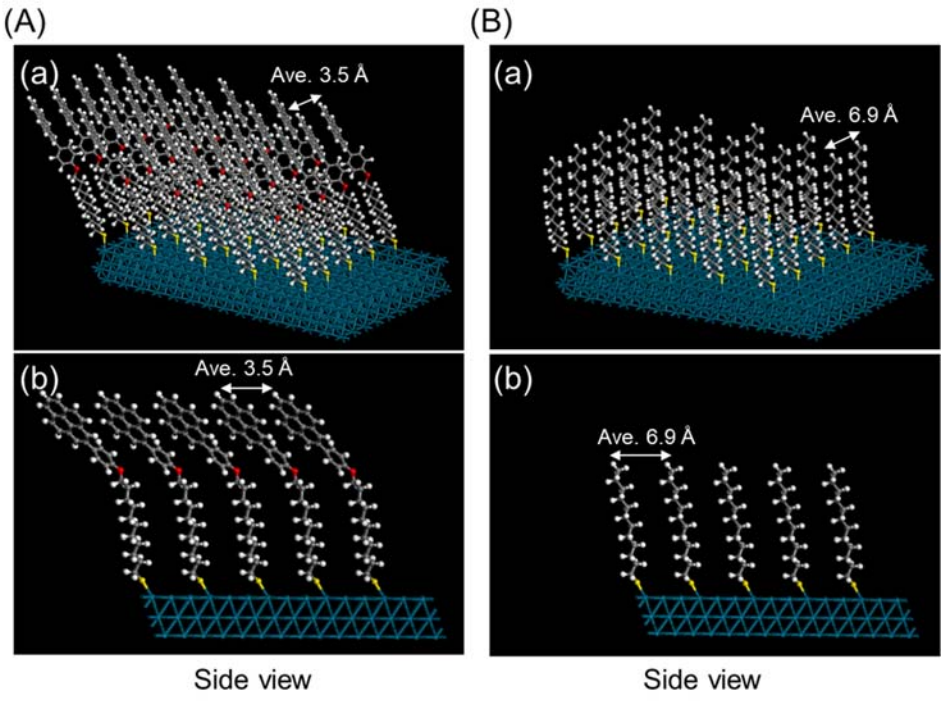

Figure 7 Geometrically optimized structures of (A) (a) pyrene-thiol ligands ($PyC_{12}SH$) immobilized Pd(111) surface cell and (b) its side view, and (B) (a) dodecanethiol ligands ($C_{12}SH$) immobilized Pd(111) surface cell and (b) its side view.

Color codes: Pd in blue, S in sulfur, O in red, C in grey, and H in white.

Competing semi-hydrogenation reaction of internal and terminal alkynes

To clarify the existence of the above-mentioned steric hindrance of pyrene-thiol ligands in $PyC_{12}S$-Pd/VC, internal alkynes were used as a substrate for the catalytic semi-hydrogenation reaction. Figure 8A summarizes the reactivity of three types of substrate (phenylacetylene, 1-phenyl-1propyne and diphenylacetylene) over $PyC_{12}S$-Pd/VC and $C_{12}S$-Pd/VC. When the terminal alkyne phenylacetylene was employed as a substrate, the reaction proceeded at nearly the same rate over $PyC_{12}S$-Pd/VC and $C_{12}S$-Pd/VC (see Figure S15A). In contrast, $PyC_{12}S$-Pd/VC exhibited a significantly lower reaction rate than that of $C_{12}S$-Pd/VC in the semi-hydrogenation of the internal alkyne 1-phenyl-1propyne (see Figure S15B), even though the molecular size of 1-phenyl-1propyne is nearly the same as that of phenylacetylene. Moreover, $PyC_{12}S$-Pd/VC showed no activity in the hydrogenation of diphenylacetylene. These specific low reactivities for internal alkynes in $PyC_{12}S$-Pd/VC can likely be attributed to the steric hindrance of pyrene groups, which restricts access by internal alkynes to the Pd NP surface.[10,60,61]

Based on the above results, a mixture of terminal and internal alkynes (phenylacetylene and diphenylacetylene) was reacted as a competing reaction over $PyC_{12}S$-Pd/VC and $C_{12}S$-Pd/VC (Figures 8Ba and 8Bb). Both terminal and internal alkynes were hydrogenated after 5 h of reaction when $C_{12}S$-Pd/VC was used. In contrast, $PyC_{12}S$-Pd/VC selectively converted the terminal alkyne phenylacetylene during 5 h of reaction; the internal alkyne diphenylacetylene was not converted completely even after the conversion of phenylacetylene reached 100%. This unique chemoselectivity in the competing semi-hydrogenation reaction over $PyC_{12}S$-Pd/VC is created by steric hindrance for internal alkynes, allowing terminal alkynes to be preferentially reacted over $PyC_{12}S$-Pd/VC.

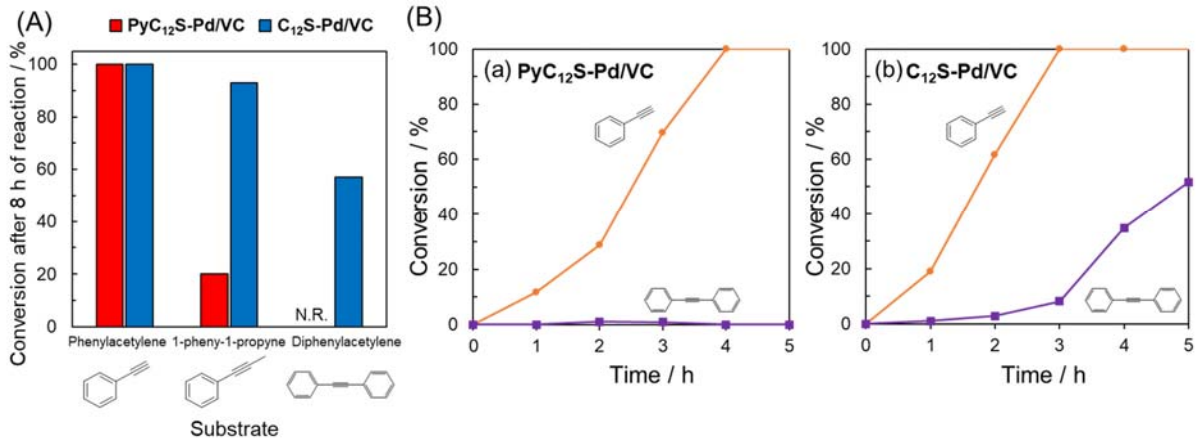

Figure 8 (A) Comparison of catalytic activity in the semi-hydrogenation of various alkynes over $PyC_{12}S$-Pd/VC and $C_{12}S$-Pd/VC. (B) Time course in the semi-hydrogenation of a mixture of terminal and internal alkynes over (a) $PyC_{12}S$-Pd/VC and (b) $C_{12}S$-Pd/VC.

Support effect on catalytic performance in semi-hydrogenation

To investigate the role of the carbon black support in $PyC_{12}S$-Pd/VC, catalysts with various supports were synthesized and assessed in the semi-hydrogenation reaction. $PyC_{12}S$-Pd NPs catalysts supported on fumed SiO_2 ($PyC_{12}S$-Pd/SiO_2) were synthesized using a procedure similar to that used for $PyC_{12}S$-Pd/VC. Figures 9A and 9B show the time courses during semi-hydrogenation of phenylacetylene over $PyC_{12}S$-Pd/SiO_2 and $PyC_{12}S$-Pd NP colloid, respectively. Unlike the case for $PyC_{12}S$-Pd/VC, the selectivity of styrene immediately decreased after the conversion of phenylacetylene reached 100% when the SiO_2 support was used. Even when $PyC_{12}S$-Pd NP colloid was used, styrene was smoothly over-hydrogenated to ethylbenzene. Therefore, the combination of pyrene-modified Pd NPs and a carbon black support is crucial for maintaining high styrene selectivity.

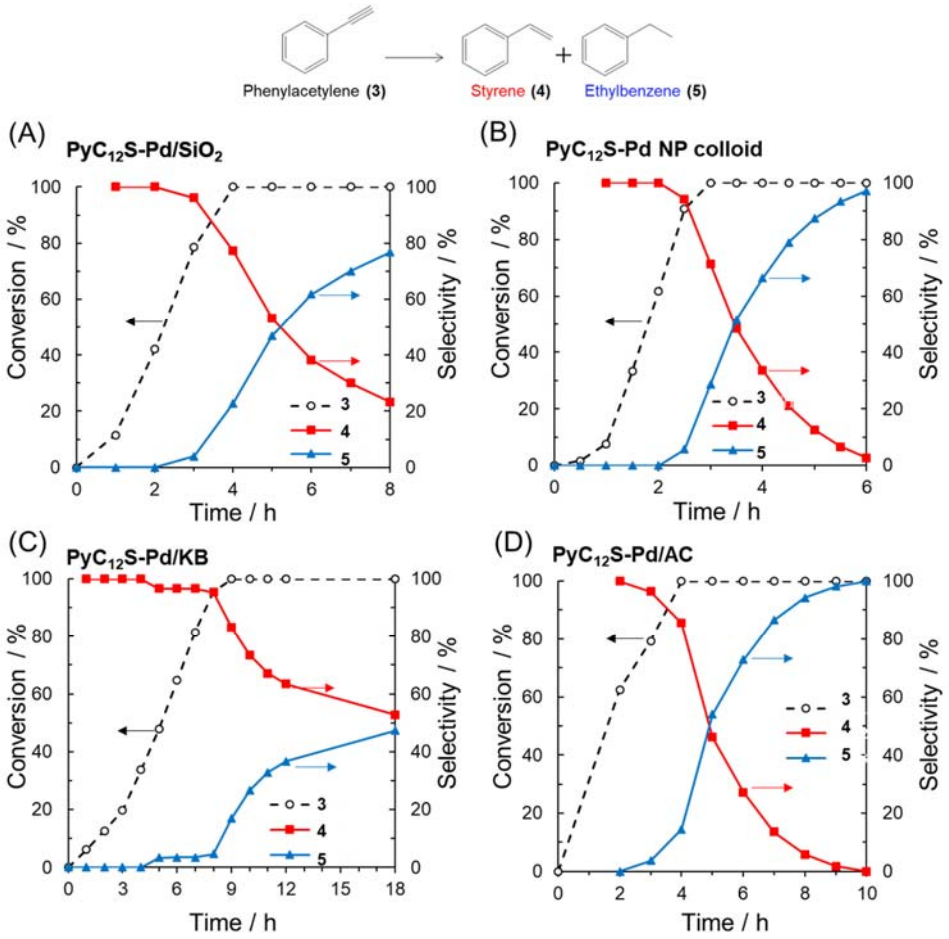

Figure 9 Time course in the semi-hydrogenation of phenylacetylene in dichloromethane over (A) $PyC_{12}S$-Pd/SiO_2, (B) $PyC_{12}S$-Pd NP colloid, (C) $PyC_{12}S$-Pd/KB and (D) $PyC_{12}S$-Pd/AC.

To elucidate the origin of the support effect on catalytic performance, the leaching rate for pyrene-thiol ligands during the catalytic reaction was estimated. Hydrogen gas was flowed for 6 h in suspensions containing $PyC_{12}S$-Pd/VC, $PyC_{12}S$-Pd/SiO_2, and $PyC_{12}S$-Pd NP colloids. The resultant suspensions were filtered to remove the catalysts and then analyzed using UV-vis measurements (Figure 10A). In contrast to $PyC_{12}S$-Pd/VC, the typical absorption band of pyrene groups at 350 nm was clearly observed when $PyC_{12}S$-Pd/SiO_2 and $PyC_{12}S$-Pd NP colloids were used, suggesting the leaching of pyrene-thiol derivatives during the reaction. Furthermore, Pd

aggregates were confirmed by TEM analysis of $PyC_{12}S$-Pd/SiO_2 taken after the reaction (Figures S10Be and S10Bf); no aggregates appeared in the fresh sample (Figure S10Bd). These results indicate that the low affinity of pyrene groups and oxide supports led to the separation of pyrene-thiol derivatives from the catalyst and the aggregation of Pd species during the reaction, which resulted in low styrene selectivity. Therefore, it is conceivable that the high catalytic performance of $PyC_{12}S$-Pd/VC is caused by the strong interaction between pyrene groups on the Pd NPs and the carbon black support. This speculation is also corroborated by the Pd 3d XPS measurement results (Figure 10B). $PyC_{12}S$-Pd/VC shows a binding energy peak of Pd $3d_{5/2}$ at 354.9 eV, which is 0.5 and 0.3 eV lower than the biding energies for $PyC_{12}S$-Pd/SiO_2 and $PyC_{12}S$-Pd NPs, respectively, indicating that the Pd species in $PyC_{12}S$-Pd/VC are in a more electron-rich state compared with the case for $PyC_{12}S$-Pd NP colloids and $PyC_{12}S$-Pd/SiO_2. In other words, charge transfer from the carbon support to Pd NPs occurs in $PyC_{12}S$-Pd/VC, supporting the existence of a strong interaction between pyrene groups on the Pd NPs and the carbon support.[35,62,63] Furthermore, our recent work revealed that more electron-rich Pd species exhibited higher catalytic activity and selectivity in the semi-hydrogenation reaction.[3,64] Therefore, the electron-richness of Pd species in $PyC_{12}S$-Pd/VC, along with the steric effect of pyrene groups, also contributes to high activity and selectivity in the semi-hydrogenation reaction.

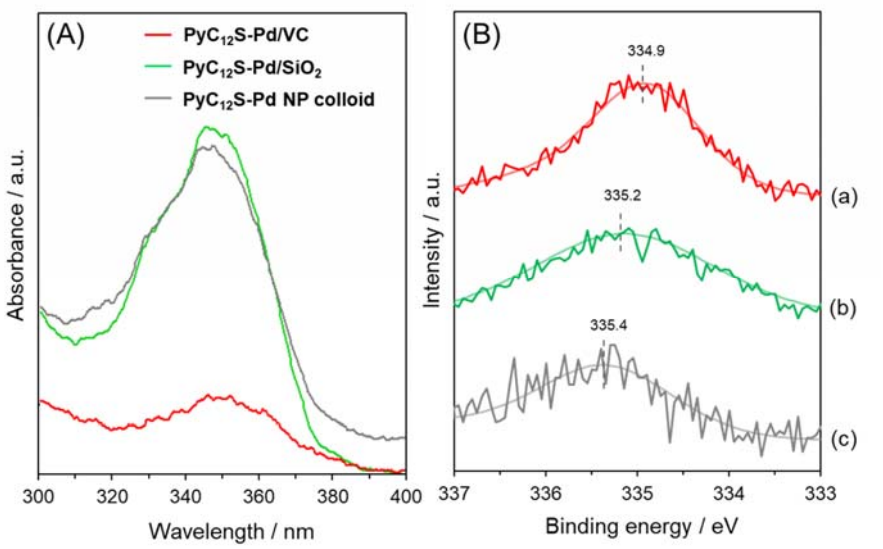

Figure 10 (A) UV-vis spectra of the filtered reaction suspension over $PyC_{12}S$-Pd/VC, $PyC_{12}S$-Pd/SiO_2, and $PyC_{12}S$-Pd NP colloid. (B) Pd $3d_{5/2}$ XPS spectra of (a) $PyC_{12}S$-Pd/VC, (b) $PyC_{12}S$-Pd/SiO_2 and (c) $PyC_{12}S$-Pd NPs.

Other types of carbon material (Ketjen black (KB) and activated carbon (AC)) were also employed for the catalytic supports, along with Vulcan XC-72 (VC), to further clarify the effect of carbon-pyrene interaction.[65] The catalysts synthesized with KB and AC are denoted as $PyC_{12}S$-Pd/KB and $PyC_{12}S$-Pd/AC, respectively. The time courses in the semi-hydrogenation of phenylacetylene over $PyC_{12}S$-Pd/KB and $PyC_{12}S$-Pd/AC are shown in Figure 9C and 9D, respectively. $PyC_{12}S$-Pd/KB maintained relatively high selectivity after the conversion reached 100% (53% styrene selectivity after 18 h reaction), although it was not as high as that obtained for $PyC_{12}S$-Pd/VC (see Figure 4B). When $PyC_{12}S$-Pd/AC was used, the styrene selectivity promptly decreased, and reached 0% after 10 h of reaction, in contrast to the case of carbon black supports (VC and KB). The XRD patterns of the three carbon supports are shown in Figure S16. The

patterns for VC, KB and AC have (002) diffraction peaks at 2θ = 24.70°, 24.65° and 23.85°, respectively. The average spacings between carbon layers (d_{002}) are calculated to be 0.360, 0.361, and 0.373 nm, respectively, which suggests that the degrees of graphitization for VC and KB are higher than that for AC. The full width at half maximum (FWHM) of the (002) diffraction peaks increases in the order of VC, KB, and AC (Table S2), which indicates that the degree of graphene stacking for VC is higher than those for KB and AC. In addition, CO gas desorption during the temperature-programmed desorption (TPD) analysis reflects the content of oxygen-containing functional groups in carbon materials.[66] As shown in Table S2, AC has a higher content of functional groups than VC and KB. Summarizing theses XRD and TPD results, the degree of graphitization of VC is highest among the three carbon materials, and AC has a relatively turbostratic structure compared to that for the carbon black supports (VC and KB), which is consistent with a previous report.[67] Considering the relationship between the reaction results and graphitic structure, a catalyst with more graphitized carbon support shows higher styrene selectivity in the reaction. These results suggest that the interaction between the pyrene groups on Pd NPs and the graphitized surface structure is essential for stable immobilization of pyrene-functionalized Pd NPs on carbon supports, and leads to high alkene selectivity and catalyst stability in the semi-hydrogenation reaction.

Conclusions

Pyrene-thiol-derivative-modified Pd NP catalysts on carbon black supports were developed for the alkyne semi-hydrogenation reaction to the corresponding alkenes. A comprehensive characterization confirmed that the prepared catalyst had highly dispersed Pd NPs

surrounded by the pyrene-thiol modifiers. In the semi-hydrogenation of terminal alkynes, high alkene selectivity was retained even after the conversion reached 100% when the prepared catalyst was used, and selectivity was higher than those of the catalyst prepared without pyrene groups and the commercial Lindlar catalyst. The solvent and substrate dependency on the catalytic reactivity and the DFT calculation study revealed that the steric effect of the pyrene groups restrict the access by the alkenes to the surface of Pd NPs, preventing the unfavorable over-hydrogenation of alkenes to alkanes. Furthermore, strong binding *via* the π-π interaction between pyrene groups on the Pd NPs and carbon black supports also plays an important role in achieving high alkene selectivity, stability, and reusability, as it suppresses leaching of pyrene modifiers from the catalysts and sintering of the Pd species during the catalytic reaction. Our study demonstrated that the rationally designed nanocomposite consisting of Pd NPs, pyrene-thiol modifiers, and a carbon support can be utilized as an efficient and stable catalyst for the semi-hydrogenation reaction.

ASSOCIATED CONTENT

Supporting Information. Detailed synthetic scheme of the pyrene-thiol ligand (Scheme S1), NMR, FT-IR and UV-vis spectra of synthesized compounds (Figure S1-S4), calculation details of the surface coverage of ligands (Figure S5), TEM images, XRD patterns, N_2 physisorption data, and XPS spectra of prepared catalysts (Figure S6-S9 and Table S1), TEM images, XRD pattern, XPS spectra of catalysts after reaction (Figure S10-S12), schematic diagrams of the ligand conformation (Figure S13), geometry optimized structures of substrates (Figure S14), time courses in semi-hydrogenation of internal alkynes (Figure S15), and XRD patterns and TPD results of carbon supports (Figure S16 and Table S2).

AUTHOR INFORMATION

Corresponding Author

*E-mail: yamashita@mat.eng.osaka-u.ac.jp. Tel./Fax: +81-(0)6-6879-7457.

ORCID

Takeharu Yoshii: 0000-0002-1869-6021

Yasutaka Kuwahara: 0000-0002-5867-6463

Kohsuke Mori: 0000-0003-3915-4528

Hiromi Yamashita: 0000-0003-1796-5776

Notes

The authors declare no competing financial interest.

ACKNOWLEDGMENT

The present work was supported by Grants-in-Aid for Scientific Research (KAKENHI No. 26220911) from the Japan Society for the Promotion of Science (JSPS). T.Y. thanks JSPS for a

Research Fellowship for Young Scientists (No. 18J20246). Y. K., K. M., and H. Y. thank the MEXT program ‘‘Elements Strategy Initiative for Catalysts & Batteries (ESICB)’’. This work was also supported in part by the Cooperative Research Program of "Network Joint Research Center for Materials and Devices” (No. 20191071). XAFS spectra were recorded at the beam line 01B1 station in SPring-8, JASRI, Harima, Japan (proposal nos. 2018B1082 and 2018B1185).

REFERENCES

(1) Jiménez-González, C.; Poechlauer, P.; Broxterman, Q. B.; Yang, B.-S.; am Ende, D.; Baird, J.; Bertsch, C.; Hannah, R. E.; Dell’Orco, P.; Noorman, H.; Yee S.; Reintjens, R.; Wells, A.; Massonneau, V.; Manley, J. Key Green Engineering Research Areas for Sustainable Manufacturing: A Perspective from Pharmaceutical and Fine Chemicals Manufacturers. *Org. Process Res. Dev.* **2011**, *15*, 900–911.

(2) Crespo-Quesada, M.; Cárdenas-Lizana, F.; Dessimoz, A. L.; Kiwi-Minsker, L. Modern Trends in Catalyst and Process Design for Alkyne Hydrogenations. *ACS Catal.* **2012**, *2*, 1773–1786.

(3) Yoshii, T.; Nakatsuka, K.; Kuwahara, Y.; Mori, K.; Yamashita, H. Synthesis of Carbon-Supported Pd–Co Bimetallic Catalysts Templated by Co Nanoparticles Using the Galvanic Replacement Method for Selective Hydrogenation. *RSC Adv.* **2017**, *7*, 22294–22300.

(4) Feng, Q.; Zhao, S.; Wang, Y.; Dong, J.; Chen, W.; He, D.; Wang, D.; Yang, J.; Zhu, Y.; Zhu, H.; Gu, L.; Li, Z.; Liu, Y.; Yu, R.; Li, J.; Li, Y. Isolated Single-Atom Pd Sites in Intermetallic Nanostructures: High Catalytic Selectivity for Semihydrogenation of Alkynes. *J. Am. Chem. Soc.* **2017**, *139*, 7294–7301.

(5) Albani, D.; Shahrokhi, M.; Chen, Z.; Mitchell, S.; Hauert, R.; López, N.; Pérez-Ramírez, J. Selective Ensembles in Supported Palladium Sulfide Nanoparticles for Alkyne Semi-Hydrogenation. *Nat. Commun.* **2018**, *9*, 1–11.

(6) Lindlar, H. Ein Neuer Katalysator Für Selektive Hydrierungen. *Helv. Chim. Acta* **1952**, *35*, 446–450.

(7) Ulan, J. G.; Kuo, E.; Maier, W. F.; Rai, R. S.; Thomas, G. Effect of Lead Acetate in the Preparation of the Lindlar Catalyst. *J. Org. Chem.* **1987**, *52*, 3126–3132.

(8) Mitsudome, T.; Takahashi, Y.; Ichikawa, S.; Mizugaki, T.; Jitsukawa, K.; Kaneda, K. Metal-Ligand Core-Shell Nanocomposite Catalysts for the Selective Semihydrogenation of Alkynes. *Angew. Chemie - Int. Ed.* **2013**, *52*, 1481–1485.

(9) Sajiki, H.; Mori, S.; Ohkubo, T.; Ikawa, T.; Kume, A.; Maegawa, T.; Monguchi, Y. Partial Hydrogenation of Alkynes Tocis-Olefins by Using a Novel Pd0–Polyethyleneimine Catalyst. *Chem. A Eur. J.* **2008**, *14*, 5109–5111.

(10) Lu, Y.; Feng, X.; Takale, B. S.; Yamamoto, Y.; Zhang, W.; Bao, M. Highly Selective Semihydrogenation of Alkynes to Alkenes by Using an Unsupported Nanoporous Palladium Catalyst: No Leaching of Palladium into the Reaction Mixture. *ACS Catal.* **2017**, *7*, 8296–8303.

(11) Vilé, G.; Almora-Barrios, N.; Mitchell, S.; Lõpez, N.; Pérez-Ramírez, J. From the Lindlar Catalyst to Supported Ligand-Modified Palladium Nanoparticles: Selectivity Patterns and Accessibility Constraints in the Continuous-Flow Three-Phase Hydrogenation of Acetylenic Compounds. *Chem. A Eur. J.* **2014**, *20*, 5926–5937.

(12) Mitsudome, T.; Yamamoto, M.; Maeno, Z.; Mizugaki, T.; Jitsukawa, K.; Kaneda, K. One-Step Synthesis of Core-Gold/Shell-Ceria Nanomaterial and Its Catalysis for Highly Selective Semihydrogenation of Alkynes. *J. Am. Chem. Soc.* **2015**, *137*, 13452–13455.

(13) Phua, P.; Lefort, L.; Boogers, J. A. F.; Vries, J. G. De. Soluble Iron Nanoparticles as Cheap and Environmentally Benign Alkene and Alkyne Hydrogenation Catalysts W. *Chem. Commun.* **2009**, 3747–3749.

(14) Nuria, L.; Crisa, V.-F. ChemComm Promoters in the Hydrogenation of Alkynes in Mixtures : Insights from Density Functional Theory W. *Chem. Commun.* **2012**, *48*, 1379–1391.

(15) Schwab, F.; Weidler, N.; Lucas, M.; Claus, P. Highly Cis-Selective and Lead-Free Hydrogenation of 2-Hexyne by a Supported Pd Catalyst with an Ionic-Liquid Layer. *Chem. Commun.* **2014**, *50*, 10406–10408.

(16) Kuwahara, Y.; Kango, H.; Yamashita, H. Pd Nanoparticles and Aminopolymers Confined in Hollow Silica Spheres as Efficient and Reusable Heterogeneous Catalysts for Semihydrogenation of Alkynes. *ACS Catal.* **2019**, *9*, 1993–2006.

(17) Yun, S.; Lee, S.; Yook, S.; Patel, H. A.; Yavuz, C. T.; Choi, M. Cross-Linked "Poisonous" Polymer: Thermochemically Stable Catalyst Support for Tuning Chemoselectivity. *ACS Catal.* **2016**, *6*, 2435–2442.

(18) Witte, P. T.; Berben, P. H.; Boland, S.; Donkervoort, J. G. BASF NanoSelect TM Technology : Innovative Supported Pd- and Pt-Based Catalysts for Selective Hydrogenation Reactions. *Top. Catal.* **2012**, *55*, 505–511.

(19) Witte, P. T.; Boland, S.; Kirby, F.; vanMaanen, R.; Bleeker, B. F.; deWinter, D. A. M.; Post, J. A.; Geus, J. W.; Berben, P. H. NanoSelect Pd Catalysts: What Causes the High Selectivity of These Supported Colloidal Catalysts in Alkyne Semi-Hydrogenation? *ChemCatChem* **2013**, *5*, 582–587.

(20) Lamey, D.; Prokopyeva, I.; Cárdenas-Lizana, F.; Kiwi-Minsker, L. Impact of Organic-Ligand Shell on Catalytic Performance of Colloidal Pd Nanoparticles for Alkyne Gas-Phase Hydrogenation. *Catal. Today* **2014**, *235*, 79–89.

(21) Marshall, S. T.; O'Brien, M.; Oetter, B.; Corpuz, A.; Richards, R. M.; Schwartz, D. K.; Medlin, J. W. Controlled Selectivity for Palladium Catalysts Using Self-Assembled Monolayers. *Nat Mater* **2010**, *9*, 853–858.

(22) Cargnello, M.; Wieder, N. L.; Canton, P.; Montini, T.; Giambastiani, G.; Benedetti, a; Gorte, R. J.; Fornasiero, P. A Versatile Approach to the Synthesis of Functionalized Thiol-Protected Palladium Nanoparticles. *Chem. Mater.* **2011**, *23*, 3961–3969.

(23) Delgado, J. A.; Benkirane, O.; Claver, C.; Curulla-Ferré, D.; Godard, C. Advances in the Preparation of Highly Selective Nanocatalysts for the Semi-Hydrogenation of Alkynes Using Colloidal Approaches. *Dalt. Trans.* **2017**, *46*, 12381–12403.

(24) Jia, C.-J.; Schüth, F. Colloidal Metal Nanoparticles as a Component of Designed Catalyst. *Phys. Chem. Chem. Phys.* **2011**, *13*, 2457-2487.

(25) Sarkar, C.; Koley, P.; Shown, I.; Lee, J.; Liao, Y. F.; An, K.; Tardio, J.; Nakka, L.; Chen, K. H.; Mondal, J. Integration of Interfacial and Alloy Effects to Modulate Catalytic Performance

of Metal-Organic-Framework-Derived Cu-Pd Nanocrystals toward Hydrogenolysis of 5-Hydroxymethylfurfural. *ACS Sustain. Chem. Eng.* **2019**, *7*, 10349–10362.

(26) Shit, S. C.; Koley, P.; Joseph, B.; Marini, C.; Nakka, L.; Tardio, J.; Mondal, J. Porous Organic Polymer-Driven Evolution of High-Performance Cobalt Phosphide Hybrid Nanosheets as Vanillin Hydrodeoxygenation Catalyst. *ACS Appl. Mater. Interfaces* **2019**, *11*, 24140–24153.

(27) Pendem, S.; Bolla, S. R.; Morgan, D. J.; Shinde, D. B.; Lai, Z.; Nakka, L.; Mondal, J. Metal-Organic-Framework Derived Co-Pd Bond Is Preferred over Fe-Pd for Reductive Upgrading of Furfural to Tetrahydrofurfuryl Alcohol. *Dalt. Trans.* **2019**, *48*, 8791–8802.

(28) Guldi, D. M.; Rahman, G. M. A.; Jux, N.; Balbinot, D.; Hartnagel, U.; Tagmatarchis, N.; Prato, M. Functional Single-Wall Carbon Nanotube Nanohybrids-Associating SWNTs with Water-Soluble Enzyme Model Systems. *J. Am. Chem. Soc.* **2005**, *127*, 9830–9838.

(29) Heidkamp, J.; Palacin, S.; Artero, V.; Jousselme, B.; Dau, H.; Guillet, N.; Fontecave, M.; Tran, P. D.; Le Goff, A. Noncovalent Modification of Carbon Nanotubes with Pyrene-Functionalized Nickel Complexes: Carbon Monoxide Tolerant Catalysts for Hydrogen Evolution and Uptake. *Angew. Chemie Int. Ed.* **2011**, *50*, 1371–1374.

(30) Bahun, G. J.; Adronov, A. Interactions of Carbon Nanotubes with Pyrene-Functionalized Linear-Dendritic Hybrid Polymers. *J. Polym. Sci. Part A Polym. Chem.* **2010**, *48*, 1016–1028.

(31) Zhang, B.; Li, X.; Li, F.; Li, Y.; Jiang, Y.; Sun, L.; Chen, L. Highly Efficient Oxidation of Water by a Molecular Catalyst Immobilized on Carbon Nanotubes. *Angew. Chemie Int. Ed.* **2011**, *50*, 12276–12279.

(32) Das, A.; Stahl, S. S. Noncovalent Immobilization of Molecular Electrocatalysts for Chemical Synthesis: Efficient Electrochemical Alcohol Oxidation with a Pyrene–TEMPO Conjugate. *Angew. Chemie - Int. Ed.* **2017**, *56*, 8892–8897.

(33) Reuillard, B.; Ly, K. H.; Rosser, T. E.; Kuehnel, M. F.; Zebger, I.; Reisner, E. Tuning Product Selectivity for Aqueous CO2 Reduction with a Mn(Bipyridine)-Pyrene Catalyst Immobilized on a Carbon Nanotube Electrode. *J. Am. Chem. Soc.* **2017**, *139*, 14425–14435.

(34) Miyabayashi, K.; Nishihara, H.; Miyake, M. Platinum Nanoparticles Modified with Alkylamine Derivatives as an Active and Stable Catalyst for Oxygen Reduction Reaction. *Langmuir* **2014**, *30*, 2936–2942.

(35) Miyabayashi, K.; Miyake, M. Metal–Support Interactions of Platinum Nanoparticles Modified with Pyrene-Functionalized Alkylamine and Improved Electrocatalytic Activity of Oxygen Reduction Reaction. *Chem. Lett.* **2017**, *46*, 707–710.

(36) Salice, P.; Gambarin, A.; Daldosso, N.; Mancin, F.; Menna, E. Noncovalent Interaction between Single-Walled Carbon Nanotubes and Pyrene-Functionalized Gold Nanoparticles in Water-Soluble Nanohybrids. *J. Phys. Chem. C* **2014**, *118*, 27028–27038.

(37) Mi, Y.; Liang, P.; Yang, Z.; Wang, D.; He, W.; Cao, H.; Yang, H. Synthesis and Co-Assembly of Gold Nanoparticles Functionalized by a Pyrene-Thiol Derivative. *RSC Adv.* **2015**, *5*, 140–145.

(38) Brust, M.; Walker, M.; Bethell, D.; Schiffrin, D. J.; Whyman, R. Synthesis of Thiol-Derivatised Gold Nanoparticles in a Two-Phase Liquid–Liquid System. *J. Chem. Soc., Chem. Commun.* **1994**, No. 7, 801–802.

(39) Delley, B. An All-Electron Numerical Method for Solving the Local Density Functional for Polyatomic Molecules. *J. Chem. Phys.* **1990**, *92*, 508–517.

(40) Delley, B. From Molecules to Solids with the DMol3 Approach. *J. Chem. Phys.* **2000**, *113*, 7756–7764.

(41) Tkatchenko, A.; Scheffler, M. Accurate Molecular Van Der Waals Interactions from Ground-State Electron Density and Free-Atom Reference Data. *Phys. Rev. Lett.* **2009**, *102*, 073005.

(42) Vitale, F.; Vitaliano, R.; Battocchio, C.; Fratoddi, I.; Piscopiello, E.; Tapfer, L.; Russo, M. V. Synthesis and Characterization of Gold Nanoparticles Stabilized by Palladium(II) Phosphine Thiol. *J. Organomet. Chem.* **2008**, *693*, 1043–1048.

(43) Corthey, G.; Rubert, A. A.; Picone, A. L.; Casillas, G.; Giovanetti, L. J.; Ramallo-López, J. M.; Zelaya, E.; Benitez, G. A.; Requejo, F. G.; José-Yacamán, M.; Salvarezza, R. C.; Fonticelli, M. H. New Insights into the Chemistry of Thiolate-Protected Palladium Nanoparticles. *J. Phys. Chem. C* **2012**, *116*, 9830–9837.

(44) Love, J. C.; Wolfe, D. B.; Haasch, R.; L, M.; Paul, K. E.; Whitesides, G. M.; Nuzzo, R. G.; Chabinyc, M. L. Formation and Structure of Self-Assembled Monolayers of Alkanethiolates on Palladium Formation and Structure of Self-Assembled Monolayers of Alkanethiolates on Palladium. *J. Am. Chem. Soc.* **2003**, *125*, 2597–2609.

(45) Gipson, K.; Stevens, K.; Brown, P.; Ballato, J. Infrared Spectroscopic Characterization of Photoluminescent Polymer Nanocomposites. *J. Spectrosc.* **2015**, *2015,* 489162.

(46) Mori, T.; Hegmann, T. Determining the Composition of Gold Nanoparticles: A Compilation of Shapes, Sizes, and Calculations Using Geometric Considerations. *J. Nanoparticle Res.* **2016**, *18*, 1–36.

(47) Murayama, H.; Ichikuni, N.; Negishi, Y.; Nagata, T.; Tsukuda, T. EXAFS Study on Interfacial Structure between Pd Cluster and N-Octadecanethiolate Monolayer: Formation of Mixed Pd-S Interlayer. *Chem. Phys. Lett.* **2003**, *376*, 26–32.

(48) San, K.; Shon, Y.-S. Synthesis of Alkanethiolate-Capped Metal Nanoparticles Using Alkyl Thiosulfate Ligand Precursors: A Method to Generate Promising Reagents for Selective Catalysis. *Nanomaterials* **2018**, *8*, 346.

(49) Gavia, D. J.; Shon, Y. S. Controlling Surface Ligand Density and Core Size of Alkanethiolate-Capped Pd Nanoparticles and Their Effects on Catalysis. *Langmuir* **2012**, *28*, 14502–14508.

(50) Navaladian, S.; Viswanathan, B.; Varadarajan, T. K.; Viswanath, R. P. A Rapid Synthesis of Oriented Palladium Nanoparticles by UV Irradiation. *Nanoscale Res. Lett.* **2009**, *4*, 181–186.

(51) Itoi, H.; Nishihara, H.; Kobayashi, S.; Ittisanronnachai, S.; Ishii, T.; Berenguer, R.; Ito, M.; Matsumura, D.; Kyotani, T. Fine Dispersion of Pt $_{4–5}$ Subnanoclusters and Pt Single Atoms over Porous Carbon Supports and Their Structural Analyses with X-Ray Absorption Spectroscopy. *J. Phys. Chem. C* **2017**, *121*, 7892–7902.

(52) Nishihara, H.; Ohtake, F.; Castro-Muñiz, A.; Itoi, H.; Ito, M.; Hayasaka, Y.; Maruyama, J.; Kondo, J. N.; Osuga, R.; Kyotani, T. Enhanced Hydrogen Chemisorption and Spillover on Non-Metallic Nickel Subnanoclusters. *J. Mater. Chem. A* **2018**, *6*, 12523–12531.

(53) Kubota, T.; Sato, H.; Uchida, T.; Kim, T. Y.; Omata, K.; Misaki, T.; Okamoto, Y.; Sugimura, T. EXAFS Characterization of Pd Catalysts for Enantioselective Hydrogenation of α-Phenylcinnamic Acid: Pretreatment Effects and Thiol Adsorption. *Catal. Letters* **2016**, *146*, 2430–2440.

(54) Sadeghmoghaddam, E.; Gu, H.; Shon, Y. S. Pd Nanoparticle-Catalyzed Isomerization vs Hydrogenation of Allyl Alcohol: Solvent-Dependent Regioselectivity. *ACS Catal.* **2012**, *2*, 1838–1845.

(55) Gavia, D. J.; Shon, Y. S. Catalytic Properties of Unsupported Palladium Nanoparticle Surfaces Capped with Small Organic Ligands. *ChemCatChem* **2015**, *7*, 892–900.

(56) Gavia, D. J.; Maung, M. S.; Shon, Y. S. Water-Soluble Pd Nanoparticles Synthesized from ω-Carboxyl-s- Alkanethiosulfate Ligand Precursors as Unimolecular Micelle Catalysts. *ACS Appl. Mater. Interfaces* **2013**, *5*, 12432–12440.

(57) Long, W.; Brunelli, N. A.; Didas, S. A.; Ping, E. W.; Jones, C. W. Aminopolymer-Silica Composite-Supported Pd Catalysts for Selective Hydrogenation of Alkynes. *ACS Catal.* **2013**, *3*, 1700–1708.

(58) López, N.; Vargas-Fuentes, C. Promoters in the Hydrogenation of Alkynes in Mixtures: Insights from Density Functional Theory. *Chem. Commun.* **2012**, *48*, 1379–1391.

(59) Bacon, G. E. The Interlayer Spacing of Graphite. *Acta Crystallogr.* **1951**, *4*, 558–561.

(60) Mastalir, Á.; Király, Z. Pd Nanoparticles in Hydrotalcite: Mild and Highly Selective Catalysts for Alkyne Semihydrogenation. *J. Catal.* **2003**, *220*, 372–381.

(61) Seth, J.; Kona, C. N.; Das, S.; Prasad, B. L. V. A Simple Method for the Preparation of Ultra-Small Palladium Nanoparticles and Their Utilization for the Hydrogenation of Terminal Alkyne Groups to Alkanes. *Nanoscale* **2015**, *7*, 872–876.

(62) Jackson, C.; Smith, G. T.; Inwood, D. W.; Leach, A. S.; Whalley, P. S.; Callisti, M.; Polcar, T.; Russell, A. E.; Levecque, P.; Kramer, D. Electronic Metal-Support Interaction Enhanced Oxygen Reduction Activity and Stability of Boron Carbide Supported Platinum. *Nat. Commun.* **2017**, *8*, 15802.

(63) Liu, B.; Wang, P.; Lopes, A.; Jin, L.; Zhong, W.; Pei, Y.; Suib, S. L.; He, J. Au-Carbon Electronic Interaction Mediated Selective Oxidation of Styrene. *ACS Catal.* **2017**, *7*, 3483–3488.

(64) Zhang, Y.; Diao, W.; Monnier, J. R.; Williams, C. T. Pd–Ag/SiO 2 Bimetallic Catalysts Prepared by Galvanic Displacement for Selective Hydrogenation of Acetylene in Excess Ethylene. *Catal. Sci. Technol.* **2015**, *5*, 4123–4132.

(65) Yoshii, T.; Nakatsuka, K.; Mizobuchi, T.; Kuwahara, Y.; Itoi, H.; Mori, K.; Kyotani, T.; Yamashita, H. Effects of Carbon Support Nanostructures on the Reactivity of a Ru Nanoparticle Catalyst in a Hydrogen Transfer Reaction. *Org. Process Res. Dev.* **2018**, *22*, 1580–1585.

(66) Bleda-Martínez, M. J.; Lozano-Castelló, D.; Morallón, E.; Cazorla-Amorós, D.; Linares-Solano, A. Chemical and Electrochemical Characterization of Porous Carbon Materials. *Carbon N. Y.* **2006**, *44*, 2642–2651.

(67) Nishihara, H.; Simura, T.; Kobayashi, S.; Nomura, K.; Berenguer, R.; Ito, M.; Uchimura, M.; Iden, H.; Arihara, K.; Ohma, A.; Hayasaka, Y.; Kyotani, T. Oxidation-Resistant and Elastic Mesoporous Carbon with Single-Layer Graphene Walls. *Adv. Funct. Mater.* **2016**, *26*, 6418–6427.

TOC GRAPHICS